Applied Radiation and Isotopes 84 (2014) 22–26

Contents lists available at ScienceDirect

Applied Radiation and Isotopes

journal homepage: www.elsevier.com/locate/apradiso

The new facility for neutron tomography of IPEN-CNEN/SP and its potential to investigate hydrogenous substances

R.M. Schoueri [a], C. Domienikan [a], F. de Toledo [a], M.L.G. Andrade [a], M.A. Stanojev Pereira [b], R. Pugliesi [a,*]

[a] *Instituto de Pesquisas Energéticas e Nucleares, Centro do Reator de Pesquisas, Av. Prof. Lineu Prestes 2242, Cidade Universitária, 05508-000 São Paulo, Brazil*
[b] *Instituto Superior Técnico, Universidade Técnica de Lisboa – Campus Tecnológico e Nuclear (IST/CTN), Estrada Nacional 10, 2686-953 Sacavém, Portugal*

HIGHLIGHTS

- A new neutron tomography facility was installed at a 5 MW nuclear research reactor.
- A tomography is obtained in 400 s with a spatial resolution of 263 μm.
- The neutron dose at the camera is only 21 μSv per tomography.
- The 3D images were enough to evaluate important aspects of some hydrogenous substances.

ARTICLE INFO

Article history:
Received 11 June 2013
Received in revised form
20 August 2013
Accepted 23 October 2013
Available online 8 November 2013

Keywords:
Neutron tomography
Neutron imaging
Scintillation screens

ABSTRACT

A new facility for neutron tomography has been installed at the IEA-R1 nuclear research reactor of IPEN-CNEN/SP. A tomography can be obtained in 400 s and the spatial resolution in the image is 263 μm. The neutron dose per tomography, in the video camera used for image capture, is only 21 μSv, assures very few damages in its CCD sensor. Some selected objects were investigated and the obtained 3D images demonstrate the capability of the facility to investigate hydrogenous substances.

1. Introduction

Neutron tomography (NT) is a powerful technique for three-dimensional visualization of hydrogenous substances like rubber, water, oil, explosives, wood, etc., even wrapped by thick metal layers. The experimental and safety conditions in different neutron sources such as nuclear reactors, spallation sources and standard particle accelerators make, in most cases, the facilities very different from each other (Saito et al., 2010; Kamiyama et al., 2010; Garbe et al., 2010). A typical NT facility is sketched in Fig. 1 and consists of a rotating table, a scintillator screen, a plane mirror and a digital video camera. Usually for the tomography, the object is rotated 360° in small angular steps of 0.9°, and 400 images are captured. Two softwares are employed, one for image reconstruction and other for 3D visualization (de Beer, 2004; Hussey et al., 2004).

In 2010 a NT facility was installed at the beam-hole (BH)-08 of the 5 MW pool-type IEA-R1 nuclear research reactor. It consists of a ^{6}LiF(ZnS) scintillator screen, a glass-based plane mirror and an ANDOR iKon-M (16 bit, 1024 × 1024 pixels, cooled CCD) video camera. The image reconstruction and the 3D visualization are performed by using the Octopus and VGStudio softwares respectively (Pereira et al., 2013). After about 6 months operation an abnormally high amount of damages in the camera's CCD, mainly produced by scattered neutrons, was detected. They appear like white spots superimposed to the image and for two reasons this amount is unexpectedly high: the camera is surrounded by appropriate neutron shielding and our old camera in use in a similar radiation environment has accumulated damages at a very lower rate. Since most of the damages are permanent, its continuous use will continuously increase them until the CCD becomes useless (Marbs and Boochs, 2006). Accordingly, the irradiations were temporarily suspended and a study to minimize the scattered neutrons at the camera was carried out, resulting in the transfer of the tomography facility to the BH14 of the same

---

* Corresponding author. Tel.: +55 11 31339993.
E-mail address: pugliesi@ipen.br (R. Pugliesi).

0969-8043/$ - see front matter © 2013 Elsevier Ltd. All rights reserved.
http://dx.doi.org/10.1016/j.apradiso.2013.10.019

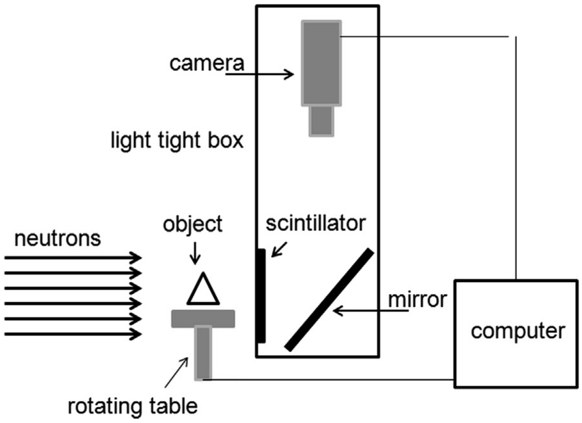

Fig. 1. Sketch of a typical NT-facility.

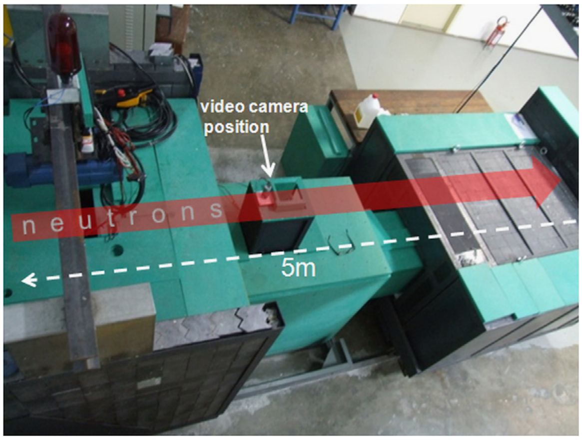

Fig. 2. Top view of the new facility.

reactor. For two reasons this BH was selected: the free space around is very adequate to implement the proposed actions and its positioning with respect to the reactor core will result in a higher neutron flux at the irradiation position.

2. The new facility for neutron tomography of IPEN-CNEN/SP

Fig. 2 shows top view of the new facility showing the main shielding at left, the central shielding inside in which the irradiations are performed, and the beam-catcher at right. This facility consists of the same scintillator screen, mirror, video camera and softwares, used in the previous one. The main implemented changes were design a collimator to reduce the neutron beam size; use diaphragms to absorb the scattered neutrons in air; improve the neutron shielding close to the camera lens by using a light transparent boron glass filter; use beam limiters to perform fine adjustments in the neutron beam size; install the video camera outside the shielding where the irradiations are performed (see Fig. 2) to minimize the backscattered neutrons to the camera. After implementing, the neutron dose rate per tomography, evaluated at the camera position was reduced by a factor 50, with respect to the value in the previous facility (see Table 1).

The following operational parameters were evaluated.

2.1. Irradiation time (Pereira et al., 2013)

Irradiation time is the required time to obtain each of the 400 images for the tomography and it was determined by means of the curve that relates the gray level – GL in the image as a function of the irradiation time – T. Several images in the interval $0.2 < T < 2$ s were captured and the results are shown in Fig. 3. Each gray level was determined by averaging the intensities of about 5000 individual pixels and the standard deviations ranged from 0.1% to 1% of the read value. A straight line was drawn to the data and it is linear until about $T = 1.4$ s. According to Octopus (2011), the images must be acquired in the linear region and must be free of saturated pixels. For the present data, such requirements are satisfied for $T = 1.0$ s, since it is ∼80% of the irradiation time that limits the linear region. During the capture, the camera's CCD is kept in a constant temperature of -20 °C, the CCD chip array was fixed to 512×512 pixels, and the reactor power was 4.5 MW.

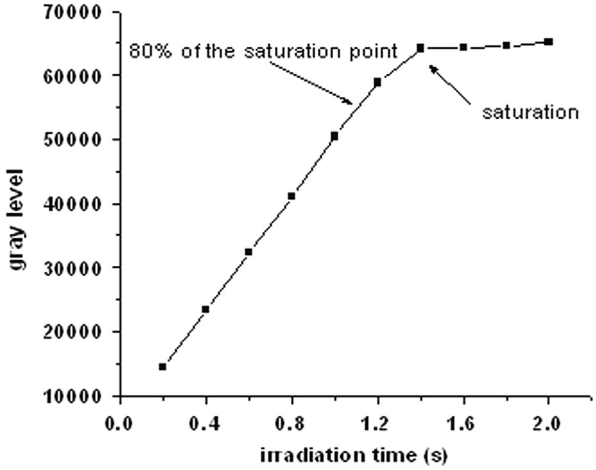

Fig. 3. Behavior of the gray level as functions of the irradiation time.

2.2. Spatial resolution (Pereira et al., 2013)

The spatial resolution is the minimal distance between objects, in such a way that they can be distinguished from each other. It is usually quoted in terms of the total unsharpness – Ut, resulting of the geometrical unsharpness – Ug from the angular divergence of the neutron beam and responsible for the penumbra in the image and of the intrinsic unsharpness – Ui from the detection system (scintillator, geometry detection, camera focusing) (Wade and Howard, 1987; Harms and Zeilinger, 1977). Since for the present facility $L/D \sim 90$ (L – source to object distance; D – inlet aperture of the neutron collimator) and taking into account the size and irregularities of the investigated objects, $0 < Ug < 550$ μm (Berger, 1965).

To evaluate the intrinsic unsharpness, firstly the best camera focus was determined. This was performed by adjusting the camera lens until the holes of the cadmium test piece, shown in Fig. 4, were sharply defined. Secondly a neutron opaque knife-edge object (gadolinium foil 127 μm) was kept in a tight contact to the scintillator and irradiated for $T \sim 1$ s. The “Edge Spread Function” – ESF, Eq. (1), was fitted to the resulting gray level distribution and the intrinsic unsharpness was evaluated by Eq. (2) (Wade and Howard, 1987).

$$ESF = p1 + p2^{*}\, a\tan(p3(x - p4)) \tag{1}$$

p_1, p_2, p_3 and p_4 are free parameters and x is the scanning coordinate.

$$Ui = 2/p3 \tag{2}$$

Fig. 5 shows the obtained result and the value for the intrinsic unsharpness was 263 ± 35 μm. This value results of the combined effect of the scintillation layer thickness of ∼400 μm that limits the resolution to ∼200 μm and of the effective pixel size of ∼254 μm, evaluated by taking into account the present camera-scintillator distance of 60 cm, a camera's field of view of 13×13 cm^2 provided by a 58 mm-f1/1.2 NIKON lens (Grünzweig et al., 2007

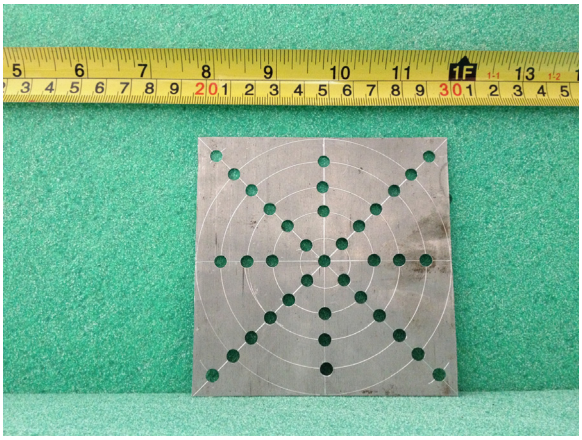

Fig. 4. Cadmium test piece for camera focusing.

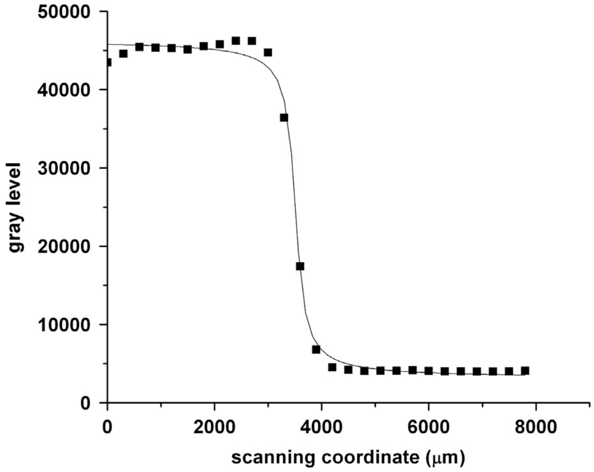

Fig. 5. Gray level distribution and the fitted ESF function.

Kardjilov et al., 2011). This image was also captured for the same camera conditions mentioned in Section 2.1.

2.3. Sensitivity to discern thickness

For a specific object it is defined as the thickness change (Δx) of the object, discernible by a gray level change (ΔGL) in the image and it was determined by means of the curve that relates "GL" as functions of the thickness "x". The objects used for such evaluation were step wedges manufactured in iron and Perspex, with thicknesses varying between 2 mm and 12 mm in steps of 2 mm. They were irradiated for $T\sim1$ s and the images were also captured for the same camera conditions mentioned in Section 2.1. The GL corresponding to each step was evaluated by averaging the gray level intensities of about 1000 individual pixels and the standard deviations range from 0.4% to 1% of the value. Fig. 6 shows the plot of "GL vs x" for both materials as well as the exponential function (Eq. (4)) fitted to the experimental data (Pugliesi and Lehmann, 2005; Hardt and von Der Roettger, 1981).

$$\mathrm{GL}=A*\exp(-B*x)+C \tag{4}$$

The discernible thickness was evaluated as the derivative of Eq. (4) (Hardt and von Der Roettger, 1981):

$$\Delta x=\Delta GL/(A*-B*\exp(-B*x)) \tag{5}$$

ΔGL is the gray level variation in the image.

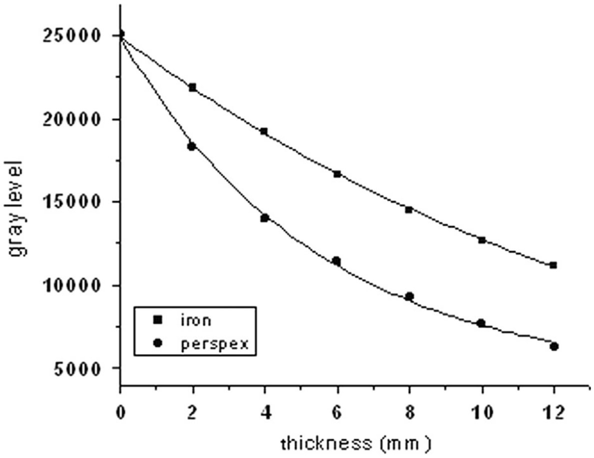

Fig. 6. Behavior of the gray level as functions of the thickness.

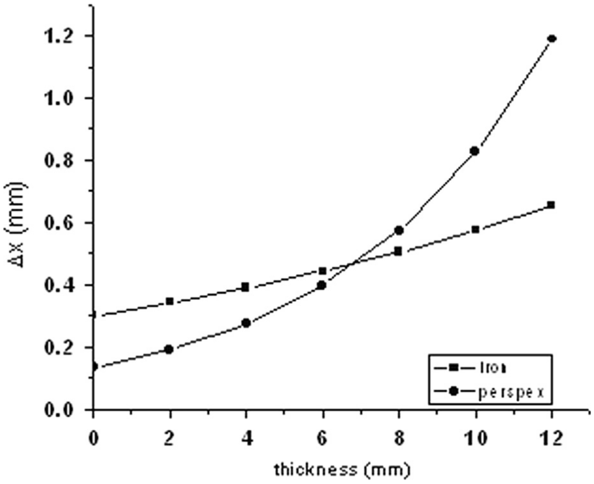

Fig. 7. Behavior of the sensitivity as functions of the thickness.

Table 1
Characteristics of the facilities installed at the BH14 and BH8.

	BH14	BH08
Flux at irradiation position (Au foil)	$8\times10^{6}\ \mathrm{n\,s^{-1}\,cm^{-2}}$	$1\times10^{6}\ \mathrm{n\,s^{-1}\,cm^{-2}}$
Mean energy	7 meV	7 meV
Irradiation time/image	1 s	8 s
Beam diameter	12 cm	15 cm
Spatial resolution	263 ± 35 μm	347 ± 26 μm
Time/tomography	400 s	4000 s
Neutron dose/tomography	21 μSv	1111 μSv

The plots of the sensitivity as a function of the thickness are shown in Fig. 7 and the minimal discernible thicknesses for the studied materials were 0.3 mm for iron and 0.13 mm for perspex. Table 1 summarizes the main characteristics of both NT facilities installed at the BH14 and at BH08.

3. Neutron images

In order to demonstrate the capability of the new facility, three selected objects, containing hydrogenous substances like, explosive, rubber and wood, were investigated. Fig. 8a shows a typical device used in aerospace engineering and consists of an explosive substance wrapped in a steel case. Fig. 8b shows a 3D neutron

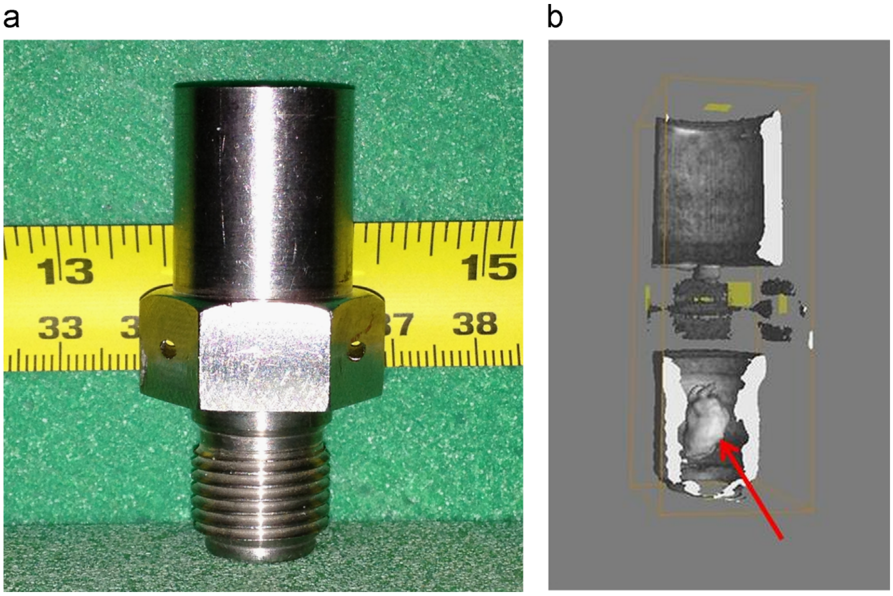

Fig. 8. (a) Device used in aerospace engineering. (b) 3D image showing the explosive substance within the steel case.

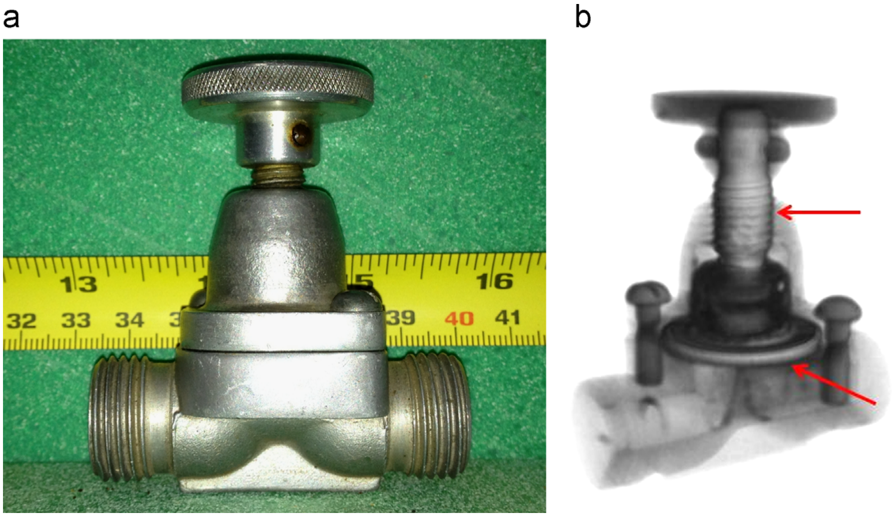

Fig. 9. (a) Valve used for water stream control. (b) 3D image showing the screw and the rubber diaphragm.

image of the device, in which the steel case was sliced and the explosive, indicated by the arrow, is clearly visible to be studied.

The second object, shown in Fig. 9a, is a standard valve usually employed for water stream control. It consists of an aluminum body inside which a rubber diaphragm is displaced up (down), as the steel screw is turned counterclockwise (clockwise), enabling (blocking) the water flow. Fig. 9b shows a 3D neutron image of the valve, in which the screw and the diaphragm, indicated by the upper and lower arrows respectively, were separated from the body, and the diaphragm is clearly visible to be studied.

The third object, shown in Fig. 10a, is a wood sample commonly used in construction, in roofs, furniture, etc. In some cases, because of propitious climate conditions (moisture and temperature) termites come into contact with the wooden material causing severe damages. Depending on the extent of the damages, it is possible to keep the wood in use by submitting it to some special chemical treatment (Essortment, 2013). Fig. 10b shows a 3D neutron image which was sliced to show the extent of the damages caused by the termites; they have eaten most of the structure of the wood sample.

4. Concluding remarks

The data presented in Table 1 demonstrate that the new NT facility installed at BH14 is an improved version of the previous one installed at BH08 and their most remarkable operational characteristics are

1. The scattered neutrons were strongly reduced leading to a decreasing by a factor 50 of the neutron dose per tomography, at the camera position.
2. The time spent per tomography is very small, only 400 s, which is 10 times smaller than the one for the previous facility and it is comparable to the one for the most important NT facilities (IAEA, 2013).
3. The intrinsic unsharpness was reduced from 347 μm to 263 μm. This is due to the improvement in the camera focus which was achieved by using the cadmium test piece shown in Fig. 4. This value is still poor when compared to the "top" facilities (IAEA, 2013). Although there are alternatives to improve it, they must be carefully considered since they lead to an increasing of the

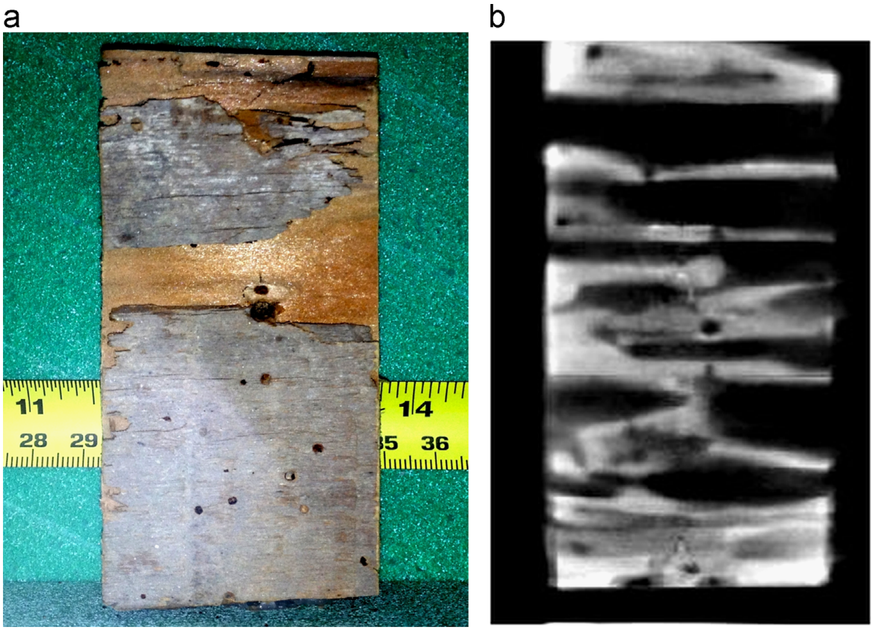

Fig. 10. (a) Wood sample used in construction. (b) 3D image showing the damages cause by the termites.

irradiation time and consequently, of the amount of damages in the CCD sensor (Pereira et al., 2013; Banhart et al., 2008; Brenizer et al., 1997).

4. The obtained 3D images shown the potential of the facility to visualize the hydrogenous substances in the selected objects. It was possible to visualize the location and distribution of the explosive substance within the steel case (Fig.8b), the positioning of the rubber diaphragm in the valve (Fig. 9b) and the degradation of the wood caused by the termites (Fig. 10b).

Acknowledgments

The authors are indebted to “São Paulo Research Foundation” – FAPESP – Brazil, for the partial financial support to this project, under the Grant 09/50261-0.

References

Banhart, J., Kardjilov, N., Manke, I., Hilger, A., Dawson, M., Kandemir, T., 2008. Neutron tomography. In: Second Australian Tomography Workshop.

Berger, H., 1965. Neutron Radiography. Methods, Capabilities and Applications. Elsevier, New York.

Brenizer, J.S., Berger, H., Stebbings, C.T., Gillies, G.T., 1997. Performance characteristics of scintillators for use in an electronic neutron imaging system for neutron radiography. Rev. Sci. Instrum. 68 (9), 3371–3379.

de Beer, F.C., 2004. Characteristics of the neutron/X-ray tomography system at the SANRAD facility in South Africa. In: Proceedings of the 5th International Topical Meeting on Neutron Radiography. Garching, Germany, July 26–30.

Essortment, 2013. ⟨http://www.essortment.com/effective-termite-treatment-45923.html⟩.

Garbe, U., Randall, T., Hughes, H., 2010. The new neutron radiography/tomography/imaging station DINGO at OPAL. In: Proceedings of the 9th WCNR. Kwa-Maritane, Pilansberg National Park, South Africa, 3–8 October.

Grünzweig, C., Frei, G., Lehmann, E., Kühne, G., David, C., 2007. Highly absorbing gadolinium test device to characterize the performance of neutron imaging detector systems. Rev. Sci. Instrum. 78 (5), 053708–053708-4.

Hardt, P., von Der Roettger, H., 1981. In: Reidl, D. (Ed.), Neutron Radiography Handbook: Nuclear Science and Technology. Dordrecht.

Harms, A.A., Zeilinger, A., 1977. A new formulation of total unsharpness in radiography. Phys. Med. Biol. 22 (1), 70–80.

Hussey, D.S., Jacobson, D.L., Arif, M., Huffman, R., Williams, R.E., Cook, J.C., 2004. New neutron imaging facility at the NIST. In: Proceedings of the 5th International Topical Meeting on Neutron Radiography. Garching, Germany, July 26–30.

IAEA, 2013. ⟨http://www-pub.iaea.org/MTCD/publications/PDF/te_1604_web.pdf⟩.

Kamiyama, T., Tsukui, D., Sato, H., Kiyanagi, Y., 2010. Accelerator based neutron tomography cooperating with X-ray radiography. In: Proceedings of the 9th WCNR, Kwa-Maritane, Pilansberg National Park, South Africa, 3–8 October.

Kardjilov, N., Manke, I., Hilger, A., Strobl, M., Banhart, J., 2011. Neutron imaging in materials science. Mater. Today 14 (6), 248–256.

Marbs, A., Boochs, F., 2006. Investigating the influence of ionizing radiation on standard CCD cameras and a possible impact on photogrammetric measurements. In: V Symposium on Image Engineering and Vision Metrology, pp. 184–189.

Octopus, 2011.Octopus8,4. ⟨http://www.inct.be/en/software/octopusS⟩.

Pereira, M.A.S., Schoueri, R.M., Domienikan, C., Toledo, F., Andrade, M.L.G., Pugliesi, R., 2013. The neutron tomography facility of IPEN-CNEN/SP and its potential to investigate ceramic objects from the Brazilian cultural heritage. Appl. Radiat. Isotopes 75, 6–10.

Pugliesi, R., Lehmann, E., 2005. Neutron-induced electron radiography using an imaging plate. Appl. Radiat. Isotopes 62 (3), 457–460.

Saito, Y., Sekimoto, S., Hino, M., Kabawata, Y., 2010. Development of neutron radiography facility for boiling two-phase flow experiment in Kyoto University Research Reactor. In: Proceedings of the 9th WCNR, Kwa-Maritane, Pilansberg National Park, South Africa, 3–8 October.

Wade, J.R., Howard, A.L., 1987. Experiments at Argonne National Laboratory. Nucl. Technol. 176, 408–419.